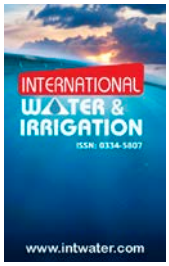

International Water and Irrigation
Volume 43 Issue 2, (2024)
ISSN: 0334-5807
Pages 133 - 148

Modeling and Active Vibration Control of Flexible Robotic Arm and Its Application in Agricultural Water Conservancy Field

Da LV[1,2] ,Chao ZHANG[1,*] , Wentao ZHAO[1], Hongbo FEI[1], Yongzhi PANG[1]

[1] School of Mechanical Engineering, Inner Mongolia University of Science and Technology, Baotou, Inner Mongolia,014030, China,

[2] Baotou Vocational and Technical College, Baotou, Inner Mongolia,014030, China,

*Corresponding author: Chao ZHANG

Abstract In order to improve the modeling and active vibration control effectiveness of flexible manipulators, this paper combines big data technology to study the modeling and active control of flexible manipulators. In addition, this article decouples the dynamic model of the flexible joint manipulator based on voltage control method, redefines the control input of the system as the voltage of the joint motor, and uses a nonlinear state observer to control the flexible link manipulator. The control strategy proposed in this article is based on a nonlinear state observer, combined with input-output control, to achieve tracking of joint angular displacement in a flexible linkage manipulator. Through experimental research, it can be seen that the big data based modeling and active vibration control research system for flexible robotic arms proposed in this paper can effectively improve the motion control effect of flexible robotic arms.

Keywords: big data; flexible manipulator; modeling; vibration; active control.

1 INTRODUCTION

The study of rigid-flexible coupled manipulators is of great significance to reduce energy consumption (especially mobile robots and aerospace robots), improve the work efficiency of manipulators and the safety of human-computer interaction. The research object relies on the rigid-flexible coupling manipulator of the multi-joint concrete pump truck. However, since the actual vibration and control of the boom of a concrete pump truck involves multiple interdisciplinary disciplines such as mechanics, hydraulics, and control, the machine-hydraulic coupling dynamics model and vibration control are very complex [1]. On the other hand, there are many commonalities in the dynamic modeling and vibration control of flexible manipulators for aerospace, engineering machinery, medical and service robots. For example, most of the manipulators in engineering applications are slender rods, which can be equivalent to the theoretical model of Euler beams [2].

Compared with the rigid arm, the elastic deformation of the arm during the movement of the flexible arm will have a great impact on the stability of the entire flexible arm system and the positioning accuracy of the end of the flexible arm, and even lead to the instability and destruction of the flexible arm system. According to the theory of elasticity, the vibration of a flexible body is a vibration system with distributed parameters and infinite dimensions. For a multi-joint flexible manipulator, its dynamic model is a highly nonlinear equation with

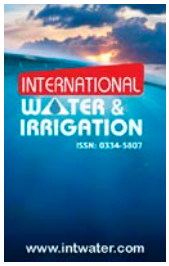

International Water and Irrigation
Volume 43 Issue 2, (2024)
ISSN: 0334-5807
Pages 133 - 148

multiple free couplings, and it is also very difficult to establish its accurate dynamic model[3]. The contact force between the flexible arm and the external environment will also seriously affect the vibration characteristics of the flexible arm when the flexible arm is operating a load or working with human-machine. Therefore, in-depth study of the dynamic characteristics of rigid-flexible coupled manipulators is of great significance for the vibration suppression and precise positioning of the end of the flexible manipulator, as well as the man-machine cooperative work of the flexible manipulator [4]. At present, most of the research on the vibration control of flexible arm is still in the stage of theoretical exploration and simulation test. The state variables of the system in the process of computer simulation can be directly obtained from the dynamic model. However, in the actual vibration control and end positioning of the flexible arm, the state feedback control law needs to be designed. Since the vibration of the flexible arm is infinite-dimensional, it is very difficult to measure and calculate the first two-order vibration modal variables of the flexible arm even through the truncation technique. difficult [5]. Essentially, the active vibration control system of the flexible arm is an underactuated system, and the vibration of the flexible arm is infinite. Due to the existence of modeling errors and sensor measurement errors, the design of multi-sensor data fusion filtering algorithm can improve the measurement accuracy of the vibration state of the flexible arm, and then improve the vibration control accuracy and end positioning accuracy of the flexible arm. The theory is of great significance to promote the practical application of flexible arm vibration state measurement and control [6]. The flexible arm moves fast, but the vibration generated during the movement makes it difficult to accurately locate the end of the manipulator, delaying subsequent operation tasks, and even the end of the manipulator cannot reach the desired working point. The vibration of the flexible arm will not only cause the fatigue damage of the manipulator system itself, but also may cause damage to the surrounding equipment or personnel [7]. Due to the complex dynamic characteristics of the flexible manipulator and the many system variables, the vibration control of the flexible manipulator is also extremely complex. Therefore, the in-depth study of the vibration control theory and method of the flexible manipulator is of great significance to the stability of the flexible manipulator system, the safety of human-computer interaction, and the improvement of its work efficiency [8].

Reference [9] uses the Ritz method to model the dynamics of two-degree-of-freedom flexible arms. The modeling accuracy of this method depends on the selection of shape functions and the series of superposition, so most of the methods are used for high-order systems of flexible arms. Truncation is performed, and only the low-order parts that play a leading role are retained. Among them, the assumed mode method (AMM, Assumedmodemethod) is a good method to select the shape function.

This paper combines the big data technology to carry out the research on the modeling and active vibration control of the flexible manipulator, so as to promote the work efficiency of the manipulator and the safety of human-computer interaction.

2 MODELING OF A FLEXIBLE JOINT ROBOTIC ARM

2.1 Research on control of flexible joint manipulator

Since the speed of the motor is inversely proportional to its torque, usually, the motor is connected to the transmission system to control its speed to obtain the desired motor torque. However, the deformation of the

International Water and Irrigation
Volume 43 Issue 2, (2024)
ISSN: 0334-5807
Pages 133 - 148

transmission system will produce flexibility at the joints, which directly affects the vibration during the operation of the flexible joint manipulator, and reduces the motion accuracy of the end effector of the manipulator.

Usually, the method to eliminate the influence of flexibility is to compensate the error caused by flexibility, that is, calibration. However, calibration requires high-precision detection methods, and the process is cumbersome, which is only suitable for adjusting a single robotic arm. In this chapter, the error caused by flexibility is compensated by active control. That is, the controller is designed to adjust the control input of the flexible joint manipulator system, and the error is compensated by dynamically adjusting the control input, so as to achieve the purpose of improving the accuracy of the flexible joint manipulator.

With the development of manipulator control theory, more and more control methods have been proposed by researchers, such as computational torque method, fuzzy control and other methods. Most of these algorithms have a common feature, that is, the motion of the manipulator is controlled by controlling the torque at the joints of the manipulator, which is also called joint torque control, as shown in Figure 1(a):

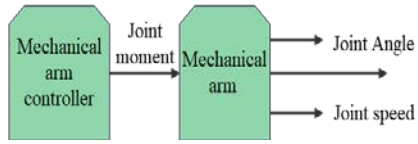

(a)Schematic diagram of joint torque control

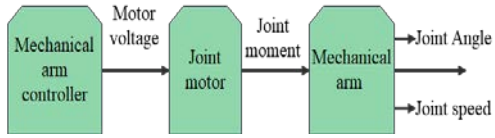

(b) Schematic diagram of voltage control

Figure 1 Schematic diagram of robotic arm control

Although this control strategy is widely used in research, its shortcomings are also quite obvious. The joint torque control method will inevitably involve solving the dynamic model of the manipulator, and the flexible joint manipulator system is a nonlinear high-order system, and the dynamic model is very complex. This also makes it difficult to apply the joint torque control method to the control of flexible joint manipulators. Therefore, in the control process of the flexible joint manipulator, the electrodynamic characteristics of the joint motor should be paid attention to. In view of the shortcomings of the joint torque control method, some scholars put forward the research on the control algorithm of the robot arm deployment based on the voltage control method.

From the analysis of the actual working conditions of the manipulator, the joint torque is the output of the joint motor, and the input of the joint motor is the voltage and current of the joint motor. In fact, the output torque can be indirectly controlled by controlling the voltage of the joint motor. Therefore, the control problem of the flexible joint manipulator can be transformed into the control problem of the joint motor. Figure 1(b) is a schematic diagram of voltage control.

International Water and Irrigation
Volume 43 Issue 2, (2024)
ISSN: 0334-5807
Pages 133 - 148

2.2 Modeling of a flexible joint manipulator

As shown in Figure 2, the joint flexibility of the flexible joint manipulator is simplified as a linear torsion spring using the spong assumption. Moreover, considering the electrodynamic characteristics of the DC motor, the dynamic model of the plane n-link flexible joint manipulator is shown in equations (1) and (2):

$$\mathbf{D}(\mathbf{q})\ddot{\mathbf{q}}+\mathbf{C}(\mathbf{q},\dot{\mathbf{q}})\dot{\mathbf{q}}+\mathbf{g}(\mathbf{q})=\mathbf{K}\left(\mathbf{r}\theta_m-\mathbf{q}\right) \quad (1)$$

$$\ddot{\theta}_m+\mathbf{B}\dot{\theta}_m+\mathbf{r}\mathbf{K}\left(\mathbf{r}\theta_m-\mathbf{q}\right)=\tau_m \quad (2)$$

Equations (1) and (2) are highly nonlinear mutually coupled, multiple-output multiple-input systems. The dynamic model of the flexible joint manipulator has two properties. First, $\mathbf{D}(\mathbf{q})$ is a positive definite symmetric and bounded matrix. Second, for the joint angle vector $\mathbf{q}\in\mathbf{R}^n$, there is $\dot{\mathbf{q}}^T[\dot{\mathbf{M}}(\mathbf{q})-2\mathbf{C}(\mathbf{q},\dot{\mathbf{q}})]\dot{\mathbf{q}}=\mathbf{0}$.

Equation (3) is the armature voltage balance equation of the joint motor:

$$\mathbf{R}\mathbf{I}_a+\mathbf{L}\dot{\mathbf{I}}_a+\mathbf{K}_b\dot{\theta}_m+\varphi=\mathbf{v} \quad (3)$$

The relationship between motor torque and motor current is as follows:

$$\mathbf{K}_m\mathbf{I}_a=\tau_m \quad (4)$$

In the equation, K_m represents the diagonal matrix of torque constants.

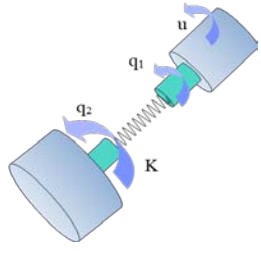

Figure 2 Flexible joint manipulator model

The voltage v of the redefined joint motor is used as the control input of the system. According to equations (1)-(4), the state space model of the flexible joint manipulator system is obtained as follows:

International Water and Irrigation
Volume 43 Issue 2, (2024)
ISSN: 0334-5807
Pages 133 - 148

$$\dot{\mathbf{x}} = \mathbf{f}(\mathbf{x}) + \mathbf{b}(\mathbf{v} - \varphi) \quad f(\mathrm{x}) = \begin{bmatrix} \mathbf{D}_2 \\ D^{-1}\left(x_1\right)\left(-g\left(x_1\right) - Kx_1 - C\left(x_1, x_2\right)x_2 + Krx_3\right) \\ x_4 \\ J^{-1}\left(r\mathbf{K}x_1 - \mathbf{r}^2\mathbf{K}x_3 - Bx_4 + K_m x_5\right) \\ -\mathbf{L}^{-1}\left(\mathbf{K}_b\mathbf{x}_4 + \mathbf{R}\mathbf{x}_5\right) \end{bmatrix}$$

$$\mathbf{b} = \begin{bmatrix} \mathbf{0} \\ \mathbf{0} \\ \mathbf{0} \\ \mathbf{0} \\ \mathbf{L}^{-1} \end{bmatrix} \quad \mathbf{x} = \begin{bmatrix} \mathbf{q} \\ \dot{\mathbf{q}} \\ \theta_m \\ \dot{\theta}_m \\ \mathbf{I}_a \end{bmatrix} (5)$$

Therefore, a decoupling model is defined, as shown in equation 6:

$$\mathbf{r}\theta_m - \mathbf{q} = \delta \quad (6)$$

In the equation, δ represents the joint flexibility term.

Substituting equation (6) into equation (2), we can get:

$$\mathbf{J}\ddot{\theta}_m + \mathbf{B}\dot{\theta}_m + \mathbf{r}\mathbf{K}\delta = \tau_m \quad (7)$$

Equations (3), (4), (6), and (7) are combined to obtain the decoupled equation:

$$\ddot{\mathbf{q}} + \mathbf{K}_a\dot{\mathbf{q}} + \mu = \mathbf{K}_v\mathbf{v} \quad (8)$$

In equation,

$$\mathbf{K}_a = \mathbf{J}^{-1}\left(\mathbf{B} + \mathbf{K}_m\mathbf{R}^{-1}\mathbf{K}_b\right) \quad (9)$$

$$\mathbf{K}_v = \mathbf{r}\mathbf{J}^{-1}\mathbf{K}_m\mathbf{R}^{-1} \quad (10)$$

$$\mu = \mathbf{r}\ddot{\delta} + \mathbf{r}\mathbf{K}_a\dot{\delta} + \mathbf{J}^{-1}\mathbf{r}^2\mathbf{K}\delta + \mathbf{K}_v\left(\mathbf{L}\dot{\mathbf{I}}_a + \varphi\right) \quad (11)$$

Equation (8) is the system dynamics equation obtained after decoupling the flexible joint manipulator system based on the voltage control method. Among them, μ represents the system uncertainty term caused by joint flexibility and external disturbances.

International Water and Irrigation
Volume 43 Issue 2, (2024)
ISSN: 0334-5807
Pages 133 - 148

2.3 Design of neural network controller

In this paper, the RBF neural network is used to approximate the system control input. The structure of the RBF neural network is shown in Figure 3:

The first layer: the input layer, and $\mathbf{s}_i(i=1,2,\cdots m)$ is the neural network input;

The second layer: the hidden layer, and it selects the Gaussian basis function,

$$\mathbf{f}_p\left(s_i\right)=\exp\left(-\frac{\left(s_i-c_{ij}\right)^2}{b_{ij}^{\ 2}}\right) \quad (12)$$

The third layer: the output layer, and y is the output of the RBF neural network.

$$y=Wf(s) \quad (13)$$

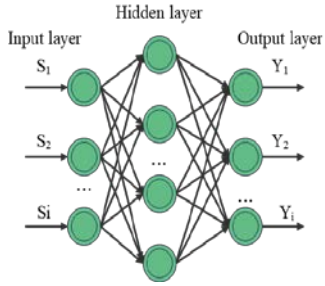

Figure 3 Schematic diagram of RBF neural network structure

In equation, $\mathbf{y}=\left[\mathbf{y}_1,\mathbf{y}_2,\mathbf{y}_3,\cdots,\mathbf{y}_k\right]^{\mathrm{T}}$, $\mathbf{f}(\mathbf{s})=\left[\mathbf{f}_p\left(\mathbf{s}_1\right),\mathbf{f}_p\left(\mathbf{s}_2\right),\cdots\mathbf{f}_p\left(\mathbf{s}_i\right)\right]^{\mathrm{T}}$, and $\mathbf{W}\in\mathbf{R}^{k\times i}$ represents the weight.

The input and output of the neural network are the joint angular displacement error $\mathbf{e}$ and the voltage $\mathbf{v}$ of the joint motor respectively, and the flexible joint manipulator can track the ideal trajectory $\mathbf{q}_d$.

$$\mathbf{e}=\mathbf{q}_d-\mathbf{q} \quad (14)$$

In equation (14), e represents the error of joint angular displacement, and $\mathbf{q}$ represents the actual joint angular displacement.

$$\dot{\mathbf{e}}=\dot{\mathbf{q}}_d-\dot{\mathbf{q}} \quad (15)$$

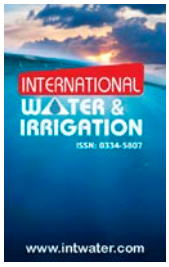

International Water and Irrigation
Volume 43 Issue 2, (2024)
ISSN: 0334-5807
Pages 133 - 148

In equation (15), $\dot{\mathbf{e}}$ represents the angular velocity error, $\dot{\mathbf{q}}_d$ represents the ideal angular velocity, and $\dot{\mathbf{q}}$ represents the actual angular velocity. The sliding mode function is defined as:

$$\mathbf{r} = \dot{\mathbf{e}} + \beta\mathbf{e} \quad (16)$$

In equation, β is a diagonal matrix.

The RBF neural network is used to approximate the control input $\mathbf{u}$.

$$u = \mathbf{W}\mathbf{f}(s) + \varepsilon \quad (17)$$

In equation (17), $\mathbf{W}$ and f(s) take the optimal values respectively, and ε is the network approximation error. The selected control rates are as follows:

$$\hat{\mathbf{u}} = \widehat{\mathbf{W}}\hat{\mathbf{f}}(\mathbf{s}) - \mathbf{u}_d \quad (18)$$

In the equation, 瀹 $f(s)$ is the estimated value of W and f(s), and u_d is the robust control term.

$$\begin{cases} \tilde{\mathbf{u}} = \mathbf{u} - \hat{\mathbf{u}} \\ \widetilde{\mathbf{W}} = \mathbf{W} - \widehat{\mathbf{W}} \\ \tilde{\mathbf{f}}(s) = f(s) - \hat{f}(s) \end{cases} \quad (19)$$

Performing a Taylor series expansion on $\tilde{f}(s)$, we get:

$$\tilde{\mathbf{f}}(s) = \mathbf{f}_c(s)\tilde{\mathbf{c}} + \mathbf{f}_b(s)\tilde{\mathbf{b}} + \mathbf{o} \quad (20)$$

In the equation, $\tilde{\mathbf{c}} = \mathbf{c} - \hat{\mathbf{c}}, \tilde{\mathbf{b}} = \mathbf{b} - \hat{\mathbf{b}}, \mathbf{o}$ is the higher-order term;

$$\mathbf{f}_c(\mathbf{s}) = \left[\frac{\partial \mathbf{f}_1}{\partial c} + \frac{\partial \mathbf{f}_2}{\partial \mathbf{c}} + \ldots + \frac{\partial \mathbf{f}_l}{\partial c}\right]\Bigg|_{c=\hat{c}} \quad (21)$$

$$\mathbf{f}_b(\mathbf{s}) = \left[\frac{\partial \mathbf{f}_1}{\partial \mathbf{b}} + \frac{\partial \mathbf{f}_2}{\partial \mathbf{b}} + \ldots + \frac{\partial \mathbf{f}_l}{\partial \mathbf{b}}\right]\Bigg|_{b=\hat{b}} \quad (22)$$

Equation (20) can be rewritten as:

$$f(s) = \hat{f}(s) + f_c(s)\tilde{c} + f_b(s)\tilde{b} + o \quad (23)$$

Equations (17), (18), (23) are substituted into $\tilde{u} = u + \hat{u}$

International Water and Irrigation
Volume 43 Issue 2, (2024)
ISSN: 0334-5807
Pages 133 - 148

$$\begin{aligned}\tilde{\mathbf{u}} &= \mathbf{W}\mathbf{f}(\mathbf{s}) + \varepsilon - \widehat{\mathbf{W}}\hat{\mathbf{f}}(\mathbf{s}) + \mathbf{u}_d \\ &= (\widehat{\mathbf{W}} + \widetilde{\mathbf{W}})\left(\hat{\mathbf{f}}(\mathbf{s}) + \mathbf{f}_c(\mathbf{s})\tilde{\mathbf{c}} + \mathbf{f}_b(\mathbf{s})\tilde{\mathbf{b}} + \mathbf{o}\right) + \varepsilon - \widehat{\mathbf{W}}\hat{\mathbf{f}}(\mathbf{s}) + \mathbf{u}_d \quad (24) \\ &= \widetilde{\mathbf{W}}\hat{\mathbf{f}}(\mathbf{s}) + \widehat{\mathbf{W}}\mathbf{f}_c(\mathbf{s})\tilde{\mathbf{c}} + \widehat{\mathbf{W}}\mathbf{f}_b(\mathbf{s})\tilde{\mathbf{b}} + \mathbf{u}_d + \delta\end{aligned}$$

In the equation:

$$\delta = \widetilde{\mathbf{W}}\mathbf{f}_c(s)\tilde{\mathbf{c}} + \widetilde{\mathbf{W}}\mathbf{f}_b(s)\tilde{\mathbf{b}} + \mathbf{W}\mathbf{o} + \varepsilon \quad (25)$$

We assume that the unknown term δ is bounded, and $\| \delta\| < \kappa$.

The parameter adaptation rate is:

$$\begin{cases}\dot{\widehat{\mathbf{W}}} = -\eta_1\left(\hat{\mathbf{f}}(\mathbf{s})\mathbf{r}^{\mathrm{T}}\right)^{\mathrm{T}} \\ \dot{\hat{\mathbf{c}}} = -\eta_2\left(\mathbf{r}^{\mathrm{T}}\widehat{\mathbf{W}}\mathbf{f}_c(\mathbf{s})\right)^{\mathrm{T}} \\ \dot{\hat{\mathbf{b}}} = -\eta_3\left(\mathbf{r}^{\mathrm{T}}\widehat{\mathbf{W}}\mathbf{f}_b(\mathbf{s})\right)^{\mathrm{T}}\end{cases} \quad (26)$$

$$\mathbf{u}_d = -\hat{\kappa}\,\mathrm{sgn}(\mathbf{r}) \quad (27)$$

$$\dot{\hat{\kappa}} = \eta_4\,\mathrm{sgn}(\mathbf{r}) \quad (28)$$

In the equation, η_1、η_2、η_3 and η_4 are constants.

The neural network controller is shown in equation (18). The neural network parameter adaptation rate (26) adjusts the weight, center value and width value online, and the robust controller is shown in equation (27) to ensure the asymptotic stability of the system.

The selected Lyapunov function is as follows:

$$\mathbf{V} = \frac{1}{2}\mathbf{r}^{\mathrm{T}}\mathbf{r} + \frac{1}{2\eta_1}\mathrm{tr}\left(\widetilde{\mathbf{W}}\widetilde{\mathbf{W}}^{\mathrm{T}}\right) + \frac{1}{2\eta_2}\tilde{\mathbf{c}}^{\mathrm{T}}\tilde{\mathbf{c}} + \frac{1}{2\eta_3}\tilde{\mathbf{b}}^{\mathrm{T}}\tilde{\mathbf{b}} + \frac{1}{2\eta_4}\tilde{\kappa}^2 \quad (29)$$

Taking the first derivative of time to equation (29), we get:

$$\dot{\mathbf{V}} = \mathbf{r}^{\mathrm{T}}\dot{\mathbf{r}} + \frac{1}{\eta_1}\mathrm{tr}\left(\tilde{\mathbf{W}}\tilde{\mathbf{W}}^{\mathrm{T}}\right) + \frac{1}{\eta_2}\dot{\tilde{\mathbf{c}}}^{\mathrm{T}}\tilde{\mathbf{c}} + \frac{1}{\eta_3}\dot{\tilde{\mathbf{b}}}^{\mathrm{T}}\tilde{\mathbf{b}} + \frac{1}{\eta_4}\tilde{\kappa}\dot{\tilde{\kappa}} \quad (30)$$

There is $\dot{\tilde{\mathbf{W}}} = \dot{\widehat{\mathbf{W}}}, \dot{\tilde{\mathbf{c}}} = \dot{\hat{\mathbf{c}}}, \dot{\tilde{\mathbf{b}}} = \dot{\hat{\mathbf{b}}}, \dot{\tilde{\mathbf{c}}} = \dot{\hat{\kappa}}$.

International Water and Irrigation
Volume 43 Issue 2, (2024)
ISSN: 0334-5807
Pages 133 - 148

When substituting equations (16), (24), (26) into (30), we get:

$$\dot{\mathbf{V}} = \mathbf{r}^{\mathrm{T}}\left[\widetilde{\mathbf{W}}\hat{\mathbf{f}}(\mathbf{s}) + \widehat{\mathbf{W}}\mathbf{f}_c(\mathbf{s})\tilde{\mathbf{c}} + \widehat{\mathbf{W}}\mathbf{f}_b(\mathbf{s})\tilde{\mathbf{b}} + \mathbf{u}_d + \delta\right] + \frac{1}{\eta_1}\mathrm{tr}\left(\widetilde{\mathbf{W}}\dot{\widetilde{\mathbf{W}}}^{\mathrm{T}}\right) + \frac{1}{\eta_2}\dot{\tilde{\mathbf{c}}}^{\mathrm{T}} + \frac{1}{\eta_3}\dot{\tilde{\mathbf{b}}}^{\mathrm{T}}\tilde{\mathbf{b}} + \frac{1}{\eta_4}\tilde{\kappa}\dot{\tilde{\kappa}}$$
$$= \mathrm{tr}\left\{\widetilde{\mathbf{W}}\left[\hat{\mathbf{f}}(\mathbf{s})\mathbf{r}^{\mathrm{T}} + \frac{1}{\eta_1}\dot{\widetilde{\mathbf{W}}}^{\mathrm{T}}\right]\right\} + \left[\mathbf{r}^{\mathrm{T}}\widehat{\mathbf{W}}\mathbf{f}_c(\mathbf{s}) + \frac{1}{\eta_2}\dot{\tilde{\mathbf{c}}}^{\mathrm{T}}\right]\tilde{\mathbf{c}} + \left[\mathbf{r}^{\mathrm{T}}\widehat{\mathbf{W}}\mathbf{f}_b(\mathbf{s}) + \frac{1}{\eta_3}\dot{\tilde{\mathbf{b}}}^{\mathrm{T}}\right]\tilde{\mathbf{b}} + \mathbf{r}^{\mathrm{T}}\left[\mathbf{u}_d + \delta\right] + \frac{1}{\eta_4}\tilde{\kappa}\dot{\tilde{\kappa}}$$
$$= \mathbf{r}^{\mathrm{T}}\left[\mathbf{u}_d + \delta\right] + \frac{1}{\eta_4}\tilde{\kappa}\dot{\tilde{\kappa}} \quad (31)$$

$$\begin{aligned}\dot{\mathbf{V}} &= \mathbf{r}^{\mathrm{T}}\left[\mathbf{u}_d + \delta\right] + \frac{1}{\eta_4}\tilde{\kappa}\dot{\tilde{\kappa}} \\ &= \mathbf{r}^{\mathrm{T}}[-\hat{\kappa}\,\mathrm{sgn}(\mathbf{r}) + \delta] + \frac{1}{\eta_4}(\kappa - \hat{\kappa})\dot{\hat{\kappa}} \\ &= \mathbf{r}^{\mathrm{T}}[-\kappa\,\mathrm{sgn}(\mathbf{r}) + \delta]\end{aligned} \quad (32)$$

$$\begin{aligned}\mathbf{r}^{\mathrm{T}}[-\kappa\,\mathrm{sgn}(\mathbf{r}) + \delta] &\le \left\|\rho^{\mathrm{T}}\right\|\delta\| - \kappa\|\,\mathbf{r}^{\mathrm{T}}\| \\ &\le \left\|\mathbf{r}^{\mathrm{T}}\right\|(\|\,\delta\| - \kappa)\end{aligned} \quad (33)$$

In the equation, $\|\,\delta\| < \kappa, \dot{\mathbf{V}} \le 0$. It can be seen that the closed-loop system is stable.

2.4 Design of Input and Output controller

In this paper, the controller is designed based on the input-output control method, and the controller is designed by redefining the output parameters of the flexible link manipulator system. For rigid manipulators, it is easy to achieve closed-loop stability of the control system by establishing a controller with joint torque and end position as the input and output of the system. The zero dynamics of a system refers to a system in which the output remains zero for a given input. The characteristics of the non-minimum phase system will make the system appear negative modulation and time delay, which will affect the stability of the system. To solve this problem, the method of redefining the output is proposed.

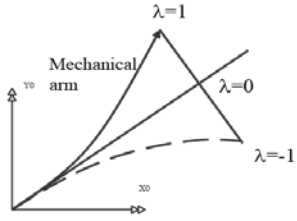

Figure 4 Output of flexible link manipulator corresponding to different values of λ

As shown in Figure 4, the output η_i of the redefinition arm i is shown in equation (34):

International Water and Irrigation
Volume 43 Issue 2, (2024)
ISSN: 0334-5807
Pages 133 - 148

$$\eta_i = \theta_i + \lambda_i \tan^{-1}\left(\frac{y_i(l_i,t)}{l_i}\right) \quad (34)$$

Among them, λ_i is a physical coefficient, $\lambda_i \in (-1,0)\cup(0,1)$. When λ_i takes different values, η_i corresponds to different outputs of the flexible link manipulator system. Compared with the control method of directly tracking the joint rotation angle, the redefinition output method can effectively control the vibration of the system.

In fact, the elastic deformation of the arm is quite small, so equation (34) can be simplified as:

$$\eta_i = \theta_i + \lambda_i \frac{y_i(l_i,t)}{l_i} i = 1,2,\cdots,n \quad (35)$$

If $\Lambda_{ij} = \frac{\lambda_i}{l_i}\left(\varphi_i(l_i,t)\right)$, the output of the flexible link manipulator system is shown in equation (36):

$$\eta = \theta + \Lambda\Lambda \quad (36)$$

Among them,

$$\Lambda = \begin{bmatrix} \Lambda_1^{\mathrm{T}}, \mathbf{0}^{\mathrm{T}}, \ldots, \mathbf{0}^{\mathrm{T}} \\ \mathbf{0}^{\mathrm{T}}, \Lambda_2^{\mathrm{T}}, \ldots, \mathbf{0}^{\mathrm{T}} \\ \mathbf{0}^{\mathrm{T}}, \ldots, \mathbf{0}^{\mathrm{T}}, \Lambda_i^{\mathrm{T}} \end{bmatrix}, \Lambda_i = \left[\Lambda_{i1}, \Lambda_{i2}, \ldots, \Lambda_{im}\right]^{\mathrm{T}} \quad (37)$$

After redefining the output of the manipulator system, the linearization of the input and output of the system can be achieved by continuous derivation of equation (36). When the joint torque τ of the system appears in the equation, the derivation is stopped. The system output η_i is used to find the second derivative with respect to time:

$$\ddot{\mathbf{i}} = \ddot{\theta} + \Lambda\ddot{\Delta} \quad (38)$$

Equation (30) is substituted into equation (38):

$$\ddot{\eta} = \Omega(\lambda, x) + \psi\left(\lambda, x_1, x_2\right)\tau \quad (39)$$

Among them,

$$\Omega = -\left(\mathbf{H}_{rr} + \Lambda\mathbf{H}_{fr}\right)\left(\mathbf{h}_r + \mathbf{g}_r\right) - \left(\mathbf{H}_{rf} + \Lambda\mathbf{H}_{ff}\right)\left(\mathbf{h}_r + \mathbf{g}_r + \mathbf{k}_{ff}x_2\right) \quad (40)$$

$$\psi = \mathbf{H}_{rr} + \Lambda\mathbf{H}_{fr} \quad (41)$$

International Water and Irrigation
Volume 43 Issue 2, (2024)
ISSN: 0334-5807
Pages 133 - 148

$$\lambda = \left[\lambda_1, \lambda_2, \ldots, \lambda_n\right]^{\mathrm{T}} \quad (42)$$

From this, the following control law can be obtained:

$$\tau = \psi^{-1}(\mathbf{v} - \Omega) \quad (43)$$

$$\mathbf{v} = \dot{\eta}_d + \mathbf{k}_v \dot{\mathbf{e}} + \mathbf{k}_p \mathbf{e} + \mathbf{k}_{d\Delta} \dot{\Delta} + \mathbf{k}_{\Delta} \Delta \quad (44)$$

Substituting equation (43) into (39), we can get:

$$v = \ddot{\eta} \quad (45)$$

Substituting equation (45) into (44), the closed-loop error dynamic equation of the system can be obtained as follows:

$$\ddot{\mathbf{e}} + \mathbf{k}_v \dot{\mathbf{e}} + \mathbf{k}_p \mathbf{e} = -\left(\mathbf{k}_{d\Delta} \dot{\Delta} + \mathbf{k}_{\Delta} \Delta\right) \quad (46)$$

2.5 Control based on nonlinear state observer

It can be seen from equation (44) that the control method proposed in this paper needs to know Δ and $\dot{\Delta}$, and the vibration of the flexible link manipulator can be suppressed by adjusting $\mathrm{k}_{\mathrm{d}\Delta}$ and k_{Δ}. The commonly used methods for measuring the vibration of the connecting rod include electrical measurement and optical measurement. The electrical measurement method is to convert the vibration signal into an electrical signal, amplify it through a charge amplifier, and then record it. The commonly used sensors are accelerometers and strain gauges. Optical measurement is to convert vibration signals into optical signals for measurement and recording, and the commonly used instruments are laser vibrometers. However, the vibration generated by the flexible link manipulator is relatively small, which is difficult to measure accurately, and adding a sensor device will change the structure of the manipulator and increase the modeling error. Therefore, a nonlinear state observer is designed to estimate the elastic vibration of the boom and its velocity.

The variables are defined as follows:

$$\varsigma_1 = \Delta \varsigma_2 = \dot{\Delta} \quad (47)$$

The state equation of equation (27) can be rewritten as follows:

$$\begin{cases} \dot{\varsigma}_1 = \varsigma_2 \\ \dot{\varsigma}_2 = H_{fr}(\theta, \varsigma_1)(\tau - \mathrm{h_r}(\mathrm{x_n}, \dot{\mathrm{x}}_\mathrm{n}) - \mathrm{g_r}(\theta, \varsigma_1)) - \\ H_{ff}(\theta, \varsigma_1)(\mathrm{h_f}(\mathrm{x_n}, \dot{\mathrm{x}}_\mathrm{n}) + \mathrm{g_f}(\theta, \varsigma_1) + \mathrm{k_{ff}}\varsigma_1) \end{cases} \quad (48)$$

The state variable $\mathbf{x}_n$ is redefined as follows:

International Water and Irrigation
Volume 43 Issue 2, (2024)
ISSN: 0334-5807
Pages 133 - 148

$$\mathbf{x}_n = \left[\theta^{\mathrm{T}}, \dot{\theta}^{\mathrm{T}}, \varsigma_1^{\mathrm{T}}, \varsigma_2^{\mathrm{T}}\right]^{\mathrm{T}} \quad (49)$$

Among them, the state variable ς_1、ς_2 is unknown, so a state observer is designed to estimate the value of ς_1、ς_2. The state equation of the flexible link manipulator can be transformed into equation (50):

$$\begin{cases} \dot{\hat{\mathbf{S}}}_1 = \hat{\zeta}_2 + \mathbf{k}_{ol}\left(\zeta_1 - \hat{\zeta}_1\right) \\ \dot{\hat{\mathbf{S}}}_2 = \mathbf{H}_{fr}\left(\theta, \mathbf{S}_1\right)\left(\boldsymbol{\tau} - \mathbf{h}_r\left(x_o, \dot{x}_o\right) - \mathbf{g}_r\left(\theta, \mathbf{S}_1\right)\right) - \\ \mathbf{H}_{ff}\left(\theta, \quad \varsigma_1\right)\left(\mathbf{h}_f\left(x_o, \dot{x}_o\right) + \mathbf{g}_f\left(\theta, \varsigma_1\right) + \mathbf{k}_{ff}\varsigma_1\right) + \\ \mathbf{k}_{o2}\left(\varsigma_1 - \hat{\zeta}_1\right) \end{cases} \quad (50)$$

In equation (50), $\hat{\mathbf{S}}_1$、$\hat{\zeta}_2$ is the estimated value of the state variable ς_1、$\mathbf{S}_2$, and $\mathbf{k}_{ol}$、$\mathbf{k}_{o2}$ represents the gain matrix of the nonlinear observer. The state variables are defined for equation (50) as follows:

$$\mathbf{x}_o = \left[\theta^{\mathrm{T}}, \dot{\theta}^{\mathrm{T}}, \varsigma_1^{\mathrm{T}}, \varsigma_2^{\mathrm{T}}\right]^{\mathrm{T}} \quad (51)$$

The observation error ς_e of the nonlinear state observer is defined as equation (52):

$$\zeta_e = \left[\left(\varsigma_1 - \hat{\zeta}_1\right)^{\mathrm{T}}, \left(\varsigma_2 - \hat{\zeta}_2\right)^{\mathrm{T}}\right]^{\mathrm{T}} \quad (52)$$

$$\dot{\zeta}_e = \mathbf{A}\mathbf{S}_e + \mathbf{B}_{\zeta} \quad (53)$$

In the equation (53):

$$\mathbf{A} = \begin{bmatrix} -\mathbf{k}_{o1}\mathbf{I} \\ -\mathbf{k}_{o2}\mathbf{0} \end{bmatrix}, \mathbf{B}_{\varsigma} = \left[\left.\frac{\partial \Gamma}{\partial \varsigma_2}\right|_{\varsigma_2 = \hat{\varsigma}_2}\left(\varsigma_2 - \hat{\varsigma}_2\right)^{\mathrm{T}} + \mathbf{O}\left(\varsigma_2^2\right)\right], \quad (54)$$

$$\Gamma = -\mathbf{H}_{fr}\left(\theta, \varsigma_1\right)\left(\mathbf{h}_r\left(x_n, \dot{x}_n\right) - \mathbf{h}_r\left(x_o, \dot{x}_o\right)\right) - \mathbf{H}_{ff}\left(\theta, \varsigma_1\right)\left(\mathbf{h}_f\left(x_n, \dot{x}_n\right) - \mathbf{h}_f\left(x_o, \dot{x}_o\right)\right)$$

3 SIMULATION ANALYSIS

The control algorithm is verified by computer simulation, and the physical parameters of the flexible joint manipulator are shown in Table 1 and Table 2:

International Water and Irrigation
Volume 43 Issue 2, (2024)
ISSN: 0334-5807
Pages 133 - 148

Table 1 Physical parameters of connecting rod

	Length (m)	Mass (kg)
Connecting rod 1	1.000	1.000
Connecting rod 2	1.000	1.000

Table 2 Physical parameters of joint motor

	Armature resistance (Ω)	Moment of inertia (kg·m^2)	Viscous damping coefficient	Joint stiffness (N·m/rad)
Joint 1	1.600	0.00020	0.0010	500.00
Joint 2	1.600	0.00020	0.0010	500.00

The torque constant of the motor is taken as 0.26. η_1=25,η_2=5,η_3=2,η_4=0.5. The ideal trajectory is:q_d=[sin(t);cos(t)].

The number of hidden layer nodes in the RBF neural network is 7, and the initial values of the center value c and the width value b are as follows:c=[−1.5,−1,−0.5,0,0.5,1,1.5;−1.5,−1,−0.5,0,0.5,1,1.5] b=[10,10,10,10,10,10,10,10,10,10; 10,10,10,10,10,10,10,10,10,10]

Figure 5 shows the computer simulation results.

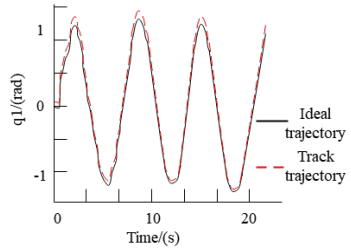

(a) Joint angle tracking of linkage 1

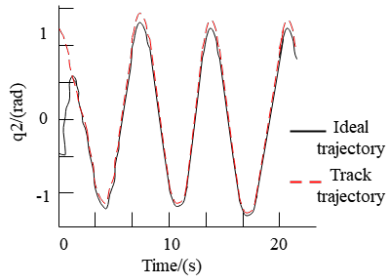

(b) Joint angle tracking of linkage 2

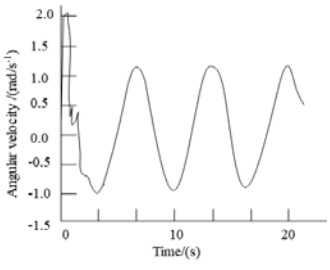

(c) The angular velocity of joint 1

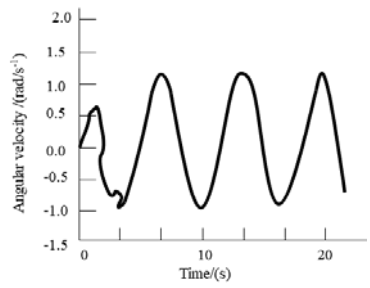

(d) The angular velocity of joint 2

International Water and Irrigation
Volume 43 Issue 2, (2024)
ISSN: 0334-5807
Pages 133 - 148

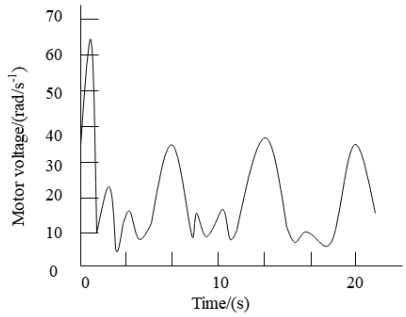

(e) Voltage input 1 of the joint motor

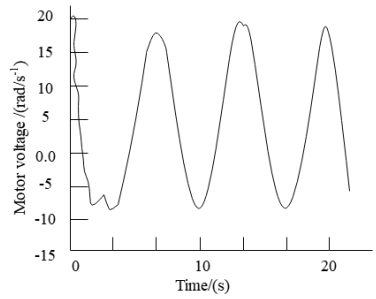

(f) Voltage input 2 of the joint motor

Figure 5 Simulation result of neural network controller

Figures a) and b) are the trajectory diagrams obtained by the neural network controller controlling the flexible joint manipulator to track the desired trajectory q_d. It can be seen from Figure a) and Figure b) that the control algorithm can track the desired trajectory within 5 seconds and respond quickly. Figure c) and Figure d) represent the angular velocity of joint 1 and joint 2, respectively, and Figure e) and Figure f) represent the voltage input of the servo motor at joint 1 and joint 2, respectively. In the process of constructing the neural network controller, it is assumed that the physical parameters of the flexible joint manipulator are completely unknown, so the parameter selection of the neural network controller is not directly related to the physical parameters of the flexible joint manipulator. Based on the voltage control method, the control input of the flexible joint manipulator system is redefined as the voltage of the joint motor. It can be seen from Figure 5 that the control input curve is relatively smooth, which is beneficial to the work of the motor.

This paper simulates in Simulink. The main function of the gtmtb toolbox is to input the feedback signal of the motor to Simulink. Simulink can call the motor position signal measured by the absolute encoder to realize closed-loop feedback control. The workflow of the experimental platform is shown in Figure 6.

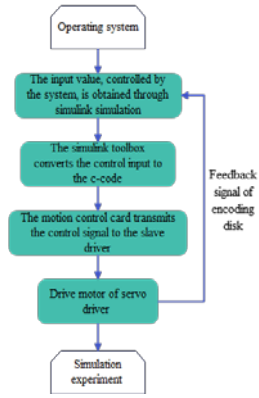

Figure 6 Workflow of the experimental platform

International Water and Irrigation
Volume 43 Issue 2, (2024)
ISSN: 0334-5807
Pages 133 - 148

The servo driver is set to the electronic gear mode, running the neural network controller constructed in Simulink to control the motion of the flexible robotic arm experimental platform. In this paper, the simulation data of the manipulator is received in Matlab, and the simulation diagram is drawn, as shown in Figure 7.

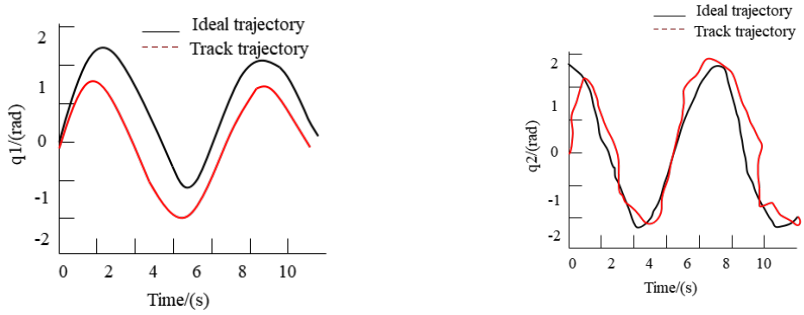

(a) Track tracking signal of joint 1 (b) Track tracking signal of joint 2

Figure 7 Trajectory tracking signal of the robotic arm

It can be seen from the above research that the modeling and active vibration control research system of flexible manipulator based on big data proposed in this paper can effectively improve the motion control effect of flexible manipulator.

4 CONCLUSION

With the rapid development of robot theory and technology, robots are applied to more and more industries, especially in the occasions with high work intensity, high precision, repetitive operation and extremely harsh environment. The rigid-flexible coupling manipulator has outstanding advantages such as light weight, large load ratio, fast movement speed, and low energy consumption. In addition, the light and flexible manipulator will be safer for humans when the human-computer interaction works together, and at the same time, it has smaller workload requirements for joint actuators, sensors, etc. This paper combines the big data technology to carry out the research on the modeling and active vibration control of the flexible manipulator, so as to promote the work efficiency of the manipulator and the safety of human-computer interaction. Through the experimental research, it can be seen that the modeling and active vibration control research system of the flexible manipulator based on big data proposed in this paper can effectively improve the motion control effect of the flexible manipulator.

Mechanical arms have broad prospects in the field of agricultural water conservancy and irrigation.

From the perspective of improving efficiency, it can achieve automated irrigation operations, quickly and accurately complete nozzle angle and height adjustments, valve switch control, etc., greatly reducing manpower input and irrigation time, and improving irrigation efficiency. In terms of precision irrigation, combined with sensor technology, robotic arms can accurately supply water based on factors such as soil moisture, crop types, and growth stages, avoiding water resource waste and excessive irrigation, improving water utilization efficiency, and promoting high-quality crop growth.

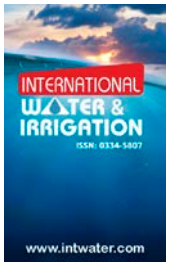

International Water and Irrigation
Volume 43 Issue 2, (2024)
ISSN: 0334-5807
Pages 133 - 148

For complex terrains and large-scale irrigation areas, the flexibility and adaptability advantages of robotic arms are highlighted, and they can operate stably in rugged mountainous orchards or vast plain farmland. Moreover, with the development of artificial intelligence and the Internet of Things, robotic arms can achieve remote control and intelligent decision-making, further promoting the development of agricultural water conservancy irrigation towards intelligence and unmanned direction, effectively solving the problem of labor shortage, and ensuring the high-quality development of agricultural irrigation.

REFERENCES

[1] Al-Kafrawi, S. Y., Al-Janadi, K. M., & Al-Bulushi, I. A. (2022). A Low-Cost IoT Based Buildings Management System (BMS) Using Arduino Mega 2560 And Raspberry Pi 4 For Smart Monitoring and Automation. *International Journal of Electrical and Computer Engineering Systems*, *13*(3), 219-236.

[2] Chen, H., Jiang, B., & Lu, N. (2018). A multi-mode incipient sensor fault detection and diagnosis method for electrical traction systems. *International Journal of Control, Automation and Systems*, *16*(4), 1783-1793.

[3] Choi, W. Y., Kang, C. M., Lee, S. H., & Chung, C. C. (2020). Radar accuracy modeling and its application to object vehicle tracking. *International Journal of Control, Automation and Systems*, *18*(12), 3146-3158.

[4] Dumitrescu, M. (2019). Marine Industry Automation Systems Simulation. *Scientific Bulletin" Mircea cel Batran" Naval Academy*, *22*(2), 7-13.

[5] Eltag, K., Aslamx, M. S., & Ullah, R. (2019). Dynamic stability enhancement using fuzzy PID control technology for power system. *International Journal of Control, Automation and Systems*, *17*(1), 234-242.

[6] Gambhire, S. J., Kishore, D. R., Londhe, P. S., & Pawar, S. N. (2021). Review of sliding mode based control techniques for control system applications. *International Journal of dynamics and control*, *9*(1), 363-378.

[7] Jansi, M. S., & Elaiyarani, M. K. (2020). IOT BASED HOME AUTOMATION SYSTEM. *Turkish Journal of Computer and Mathematics Education (TURCOMAT)*, *11*(3), 2246-2253.

[8] Kryukov, O. V., Gulyaev, I. V., & Teplukhov, D. Y. (2019). Method for stabilizing the operation of synchronous machines using a virtual load sensor. *Russian Electrical Engineering*, *90*(7), 473-478.

[9] Liang, W., Zheng, M., Zhang, J., Shi, H., Yu, H., Yang, Y., ... & Zhao, X. (2019). WIA-FA and its applications to digital factory: A wireless network solution for factory automation. *Proceedings of the IEEE*, *107*(6), 1053-1073.